

Hydrol. Earth Syst. Sci. Discuss., 11, C5692–C5694, 2014  
www.hydrol-earth-syst-sci-discuss.net/11/C5692/2014/  
© Author(s) 2014. This work is distributed under  
the Creative Commons Attribute 3.0 License.

Hydrology and  
Earth System  
Sciences

Open Access

Discussions

**Interactive comment on “Understanding NMR relaxometry of partially water-saturated rocks”**

**by O. Mohnke et al.**

Received and published: 15 December 2014

**Responses to specific reviewer comments**

**Anonymous Referee #1**

**General**

Figure 2b) With regard to the initial condition, where does the shift to slower relaxation times (96-89) in the beginning comes from?

We checked the data and discovered an error in our data plot processing, mixing up data entries from different samples of the study. We exchanged figure 2b with the correct T1 distribution results.

Figure 8, 9 and 11.

Where does the difference in the surface relaxivity parameter  $10^{-5}$  m/s to  $10^{-10}$  m/s comes from?

No difference, corrected the typo in units m vs us

Page 12698

Line 4 the NMR signal amplitude needs to be extrapolated to be proportional to porosity  
Changed to ‘initial signal amplitude’

Line 5-7 state that “[. . .] the relationship between pore size and NMR relaxation depends on pore shape [. . .]” whereas in the conclusions on page 12712 line 12 -14 “The NMR relaxation time depends on the surface-to-volume ratio (not on pore shape) [. . .]” is written. Please clarify, this seems contradictory.

We agree, and clarified this statement, to avoid confusion between NMR behavior at fully and partially saturation

Page 12705

Line 6 The whole paragraph needs to be more clear since the loss of phase coherence is a T2 issue and therefore not related to T1 as Eq. 8 states.

Clarified and removed reference to T2 phase coherence effects

## Technical

Figures should be larger and printed in high resolution, they are hard to read in terms of font size and color

Figures image files are basically all in a good resolution, but seemingly were degraded during pdf conversion. We will possibly need check on that with HESS layouter

Figure 8b and c) decay time? T1 or T2?

Figure 10) decay time? T1 or T2?

Added 'longitudinal' magnetization in the respective captions in Fig 8, 9 and 10 to clarify (it is already referred to the NMR relaxation as T1)

Figure 8. Surface relaxivity has a wrong unit

Corrected

Figure 14) decay time? T1 or T2?

Corrected the plots to show T1 buildup signal behavior and corrected and clarified the caption

Figure 14. Amplitude of what? T1 or T2? Is this the extrapolated amplitude?

Clarified, that it is related to T1; Note, as we show simulated data we can directly calculate initial amplitude  $M_0(t=0)$  similar to measured NMR data the integral of inverted T1 distributions yields the initial amplitude.

Page 12698

Line 25 delete "the"

Corrected

Page 12699

Line 6-9 the extrapolated signal amplitudes are proportional

Changed to 'initial signal amplitudes'

Page 12700

Line 22 insert blank between "and water"

Corrected

Page 12701

Line 25 air is not a fluid, I suggest to use the phrase "non-wetting phase" instead of Fluid

Changed to "non-wetting phase" (also changed the other occurrence on page12702, L2)

Page 12705

Line 11 I assume that you mean that the [ . . ]molecules diffuse at the wall [ . . ]- please clarify

Changed to "diffuse to at the pore walls"

## S. Costabel (Referee)

stephan.costabel@bgr.de

General comments:

The manuscript suggests the use of capillaries with triangular cross-sections for interpreting NMR relaxometry data of partially saturated rocks. Using this kind of pores, one accounts for remaining water menisci during de-saturation trapped by capillary forces in the corners of the triangle. After explaining the known properties of such pore systems regarding drainage/imbibition and the physical relationship between pore pressure and remaining water content, the NMR response of the water menisci is analytically derived and verified by numerical simulations. The NMR properties of single capillaries with triangular cross-section as well as a corresponding bundle of capillaries (pore size distribution) are analyzed and compared to usual circular capillaries. Unfortunately, the authors show only one real NMR data example (Rotliegend sandstone) to motivate the necessity of their study. Therefore, I am afraid that the relevance of this paper might be questioned by the community. However, I know from own experience with loose sediments that the phenomenon of occurring relaxation regimes for  $S < 1$  outside the original relaxation time distribution at  $S = 1$  can very often be observed, even with pure sand. I urgently suggest to show more own data or refer to literature with further data examples for motivation (e.g. Costabel, 2011; Bird et al., 2005; Jäger et al. 2009).

**We added additional references (also, see comments below)**

I suggest to accept the paper after major revisions.

The step from single pore to pore size distribution must be explained, analyzed and discussed more in detail. I would be glad to see a figure similar to Fig. 1 (de-saturation for the bundle of circular capillaries) also for the distribution of triangles.

**Included figure with desaturated triangular pore size distributions and added discussion in text**

Furthermore, the critical role of hysteresis and its representation in the simulated NMR data is not worked out adequately, although the authors mention this in the Summary/Conclusions section as key feature of their approach (P 12711 L 17).

**We added additional figures and included a paragraph to better illustrate and clarify the observed hysteresis behavior.**

I doubt that hysteresis effects can be observed unambiguously using NMR relaxometry.

**Agreed, possibly a very challenging experiment to demonstrate. Other complementary data, a priori information/assumptions and/or model constraints would be required. However, the main focus here is on introducing and promoting a basic model towards improving the understanding of NMR behavior on partially saturated rocks or soil.**

However, I believe that the key feature of triangular pore spaces is the exact description of the physical relationship between remaining water content, pore pressure and permeability/hydraulic conductivity (e.g. Tuller and Or, 2001).

Using this relationship for interpreting NMR data would be a clear benefit and this manuscript has the potential to show the way how this can be done.

Best regards, Stephan Costabel

Additional references:

Costabel, S.: Nuclear magnetic resonance on laboratory and in field scale for estimating hydraulic parameters in the vadose zone, PhD thesis, Berlin University of Technology, 2011. ([opus4.kobv.de/opus4-tuberlin/files/3173/costabel\\_stephan.pdf](http://opus4.kobv.de/opus4-tuberlin/files/3173/costabel_stephan.pdf))

Added above reference and additional comments regarding in the text (see below)

Bird, N. R. A., Preston, A. R., Randall, E. W., Whalley, W. R., and Whitmore, A. P. (2005). Measurement of the size distribution of water-filled pores at different matric potentials by stray field nuclear magnetic resonance. *European Journal of Soil Science*, 56:135143.

Jaeger, F., Bowe, S., van As, H., and Schaumann, G. E. (2009). Evaluation of  $^1\text{H}$  NMR relaxometry for the assessment of pore size distribution in soil samples. *European Journal of Soil Science*, 60:1052 – 1064.

Added above references

Specific comments:

P 12699 L 20: Include (2006) after citing Al-Mahrooqi et al.  
corrected

P 12700 L 22: Include a space after “and”  
corrected

P 12700 L 26: Costabel (2011) analytically derived the NMR response of a single water meniscus for the first time (for an arbitrary opening angle and for the fast diffusion regime, Costabel, 2011, Pages 33 – 38). It would be fair to cite this work, even if it is (only?!) a part of the PhD thesis and not published as a peer reviewed paper. Costabel (2011) analyzed the relationship between mean relaxation time (= single angular pore system) and saturation degree (Costabel, 2011, Pages 33 – 41). He also concluded that, when considering capillaries with angular cross-sections, new relaxation regimes will occur during de-saturation that might exceed the relaxation time distribution at  $S=1$  towards smaller relaxation times (Costabel, 2011, Page 61).

Agreed, this goes without any questions! We have cited this work accordingly.

P 12701 L 2: I could not figure out what you mean by “. . . the simulated signals are tested using synthetic pore size distributions.” Do you really test the simulated signals? As I understand, you simulate signals based on synthetic pore size distributions.

We clarified the sentence

P 12701 L 20: “. . . gravity forces are weak.” Actually, these are neglected.

### Added comments in the text

P 12705 L 11 - 14: I suggest to include the term “fast diffusion” anywhere in this sentence.

P 12708 L 4: The term “fast diffusion” is referred to here for the first time without any further explanation. Please introduce it first (e.g. at P 12705 L 11-14).

C5735

Introduced fast diffusion term in 12705, L11ff

P 12709 L5: Fig.11 has no subplot “a”.

Deleted the reference to Fig.11a

P 12709 L9: Include “partially saturated” before “system of pores”

Corrected

P 12709 L 18 to P 12710 L 7: I do not understand the necessity of combining the analyses of the drainage/imbibition behavior of the angular pore system and the NMR response of that system in this passage. The focus jumps from Fig. 14 to Fig. 13, then back to 14 and back again to 13, before Fig. 14 is analyzed in detail, which is quite confusing. Finally, no effects of hysteresis can be observed in the simulated NMR data in Fig.14. Indeed, I would not expect that any drainage/imbibition behavior can be made visible using these NMR simulations. Therefore, I suggest to compare and discuss the hysteresis effects of the pore systems earlier, e.g. after introducing the de-saturation behavior of the single pores in Fig. 4 and Fig. 5. Here, in section 2.3 you should focus the discussion on the NMR responses at partial saturation only. If you do not agree, please explain more in detail how the hysteresis effects influence the NMR data and discuss how this influence can possibly be used in future interpretation schemes. I expect that there is a natural ambiguity between drainage and imbibition that cannot be resolved by NMR relaxometry.

We added additional figures and rearranged paragraphs so for a more consistent read without jumping to better address these items (also, see our response above)

P 12710 L 8 ff: In addition to my concerns above, some important details on the simulations in Fig.14 are missing. What are the properties of the underlying pore size distributions for the three cases?

What are the values for  $T_{bulk}$  and surface relaxivity.

Why did you choose the T2 relaxation here in contrast to the T1 simulations in Fig. 8 and 9? Possibly, this information should be introduced together with Fig.12, but Fig.12 is not mentioned in the text at all. Seems to be a lognormal distribution: what are the values for the mean and the standard deviation?

Parameters for pore size distribution were included and changed the figures to be consistent with the previous discussion of NMR T1 relaxation. Also, the order of figures was adjusted accordingly.

P 12710 L 25: Regarding the assumption of pore size distributions based on triangular capillaries, there is a principle problem occurring during de-saturation. The pore system is considered to be a bundle of triangular capillaries and each capillary has its individual size, but all are similar in shape. After the snap-off, the contribution of each capillary to the NMR relaxation behavior is identical, even if they are originally different

in size. This is because the de-saturation is controlled by the pressure, which determines the curvature of the arc meniscus. Following the concept of reduced geometry all de-saturated triangles with their remaining water in the corners look the same. Consequently, at some point during de-saturation, i.e., if the air has entered all capillaries of the pore system, only one single relaxation time is left for the case of the equilateral triangles (Fig. 14b) or three relaxation times for the case of the right-angled triangles (Fig. 14c). Strictly speaking, the assumption of a relaxation time distribution is no longer valid at this point. This is a conceptual problem and must be discussed at the end of this section.

Agreed, we are aware of this inherent behavior of a single (or n) corner related discrete decay times. Seemingly, becoming somewhat 'professionally blinkered' of this 'obvious' behavior we did not include this particular point in our initial discussion. We have thankfully taken up on that comment and added a figure and discussion of this behaviour.

This feature is of course not captured in the typical inverse modeling approach for NMR lab/log data we used here. We also tried to address this accordingly in discussion and conclusion It is intended to implementing this concept an adapted future inversion scheme mentioned as part of our outlook.

P 12711 L 17 – 19: A discussion is missing on how the hysteresis behavior is encoded in the NMR data. This is not obvious from Fig. 14. Please see also my comment on P 12709 L 18 to P 12710 L 7.

Include NMR related hysteresis plots in a consolidated figure (Fig. 15)

P 12711 L 12: On the statement “. . .triangular pores strongly influence . . . hydraulic properties”. Tuller and Or (2001) derived the hydraulic conductivities for different crossections of capillaries, also for the equilateral triangle. What relationship between shape/size of the triangle and saturated hydraulic conductivity must be expected? Such information would strengthen your statement a lot.

We added a paragraph and discussed this relationship

P 12711 L 22 - 25: You should explain in detail what benefits are expected of such an inversion scheme compared to the classical approach of using circular capillaries. What are the shortcomings of existing approaches for partial saturation if the remaining water menisci remain unconsidered?

We tried to point out and list possible benefits, e.g. NMR inversion on partially saturated rocks when estimating surface relaxivity or predicting relative permeability from laboratory or borehole data

# 1 Understanding NMR relaxometry of partially water-saturated rocks

2 O. Mohnke, R. Jorand, C. Nordlund, N. Klitzsch

3 Institute for Applied Geophysics and Geothermal Energy (GGE), E.ON Energy Research  
4 Center (E.ON ERC), RWTH Aachen University, Mathieustrasse 10, 52074 Aachen

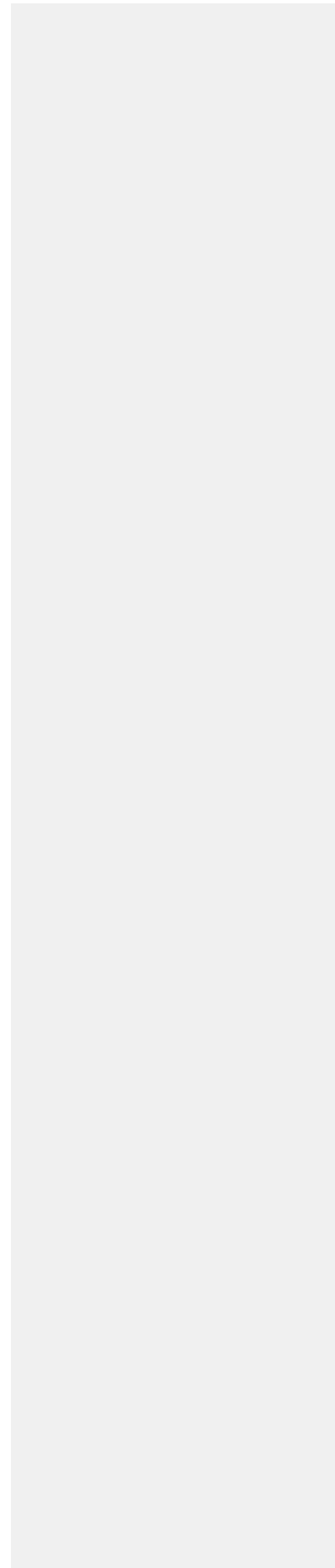
5

## 6 Abstract

7 Nuclear Magnetic Resonance (NMR) relaxometry measurements are commonly used to  
8 characterize the storage and transport properties of water-saturated rocks. These assessments  
9 are based on the proportionality of NMR initial signal amplitude and relaxation time to  
10 porosity (water content) and pore size, respectively. ~~Herein, The relationship between pore~~  
11 ~~size and NMR relaxation time depends on~~ pore shapes, ~~which is~~ are usually assumed to be  
12 spherical or cylindrical. However, the NMR response at partial water saturation for natural  
13 sediments and rocks may differs strongly from the responses calculated for spherical or  
14 cylindrical pores, because these pore shapes cannot account for water menisci remaining in  
15 the corners of de-saturated angular pores. Therefore, we consider a bundle of pores with  
16 triangular cross-sections. We introduce analytical solutions of the NMR equations at partial  
17 saturation of these pores, which account for water menisci of de-saturated pores. After  
18 developing equations that describe the water distribution inside the pores, we calculate the  
19 NMR response at partial saturation for imbibition and drainage based on the deduced water  
20 distributions.

21 For this pore model, NMR amplitude and NMR relaxation time at partial water saturation  
22 strongly depend on pore shape even so the NMR relaxation time at full saturation only  
23 depends on the surface to volume ratio of the pore. The pore-shape-dependence at partial  
24 saturation arises from the pore shape and capillary pressure dependent water distribution in  
25 pores with triangular cross-sections. Moreover, we show the qualitative agreement of the

26 saturation dependent relaxation time distributions of our model with those observed for rocks  
27 and soils.





## 28 **1 Introduction**

29 Understanding multi-phase flow processes in porous rocks and soils is vital for addressing  
30 a number of problems in ~~the~~ geosciences such as oil and gas recovery or vadose zone  
31 processes, which influence groundwater recharge and evaporation. Effective permeability,  
32 which is defined as the permeability of a fluid in presence of another fluid, is the decisive  
33 parameter for fluid transport, and depends on fluid saturation, wetting condition, and pore  
34 structure. In addition, saturation history influences the fluid content and the effective  
35 permeability (for a specific pressure), which are different for imbibition and drainage.

36 A method considered suitable for determining water content of rocks non-invasively is  
37 nuclear magnetic resonance (NMR), because the NMR initial signal amplitudes are directly  
38 proportional to the hydrogen content in the pore space, and the NMR relaxation times are  
39 linked to the size of the water-containing pores in the rock. In a two-phase system of water  
40 and air only the water contributes to the NMR signal response. Therefore, NMR is widely  
41 used for estimating transport and storage properties of rocks and sediments (Kenyon, 1997;  
42 Seevers 1966; Fleury et al., 2001; Arnold et al., 2006).

43 In recent years, several researchers have studied the relationship between NMR and  
44 multiphase flow behavior on the pore scale to better understand and infer the storage and  
45 transport properties of partially saturated rocks or sediments (e.g., Chen et al., 1994; Liaw et  
46 al. 1996; Ioannidis et al., 2006; Jia et al., 2007; Al-Mahrooqi et al., 2006; Costabel and  
47 Yaramanci, 2011, 2013; Talabi et al., 2009). As an extension of this research, we study the  
48 relationship between the water distribution inside the pores of a partially saturated rock and  
49 the system's NMR response by using bundles of pore with triangular cross-sections. While  
50 Al-Mahrooqi et al. (2006) used a similar modeling approach to infer the wettability properties  
51 in oil-water systems, this study investigates the evolution of the NMR relaxation-time spectra  
52 during drainage and imbibition. For this purpose, we consider a capillary pore ensemble that

53 is partially saturated with water and air. Traditionally, the pores within this ensemble are  
54 assumed to have a cylindrical geometry. Depending on pressure, cylindrical capillaries are  
55 either water- or air-filled and thus they either contribute to an NMR response or they do not.  
56 Consequently, the NMR relaxation times of partially water-saturated capillary pore bundles  
57 always remain subsets of the fully saturated system's relaxation-time distribution, i.e., they  
58 are a function inside the envelope of the distribution curve at full saturation (see Fig. 1-a).  
59 However, in porous rocks, which are formed by the aggregation of grains, the pore geometry  
60 is usually more complex (Lenormand et al., 1983; Ransohoff and Radke, 1987; Dong and  
61 Chatzis, 1995) and may exhibit angular and slit-shaped pore cross-sections rather than  
62 cylindrical capillaries or spheres (Fig. 2a). For example, in tight gas reservoir rocks Desbois  
63 et al. (2011) found three types of pore shapes that are controlled by the organization of clay  
64 sheet aggregates: i) elongated or slit-shaped, ii) triangular, and iii) multi-angular cross-  
65 sections. The relaxation-time distribution functions derived from NMR measurements for  
66 such partially saturated rocks are frequently found to be shifted towards shorter relaxation  
67 times outside the original envelope observed for a fully saturated sample, (Fig. 2b) (e.g.,  
68 Applied Reservoir Technology Ltd., 1996; [Bird, et al., 2005](#); [Jaeger et al., 2009](#); Jorand et  
69 al., 2010; Stingaciu, 2010a,b; [Costabel, 2011](#)).

70 In angular pores, water will remain trapped inside the pore corners even if the gas entry  
71 pressure is exceeded. Standard NMR pore models that assume cylindrical or spherical pore-  
72 ensembles (e.g., Kenyon, 1997), however, do not account for such residual water (Blunt et  
73 al., 2002; Tuller et al., 1999; Or and Tuller, 2000; Tuller and Or, 2001; [Thern, 2014](#)). To  
74 overcome this limitation, we [adopt an NMR modeling approach initially proposed and](#)  
75 [discussed by Costabel \(2011\) and present](#) numerical simulations and analytical solutions of  
76 the NMR equations for partially saturated pores with triangular cross-sections to quantify  
77 NMR signal amplitudes and relaxation times. The NMR response of a triangular capillary

78 during drainage and imbibition depends on the water distribution inside the capillary, which  
79 is subject to pore shape and capillary pressure. Thus, in the next chapter we present the  
80 relationship between capillary pressure and water distribution inside cylindrical and  
81 triangular pore geometries during drainage and imbibition. For this purpose, the reduced  
82 similar geometry concept introduced by Mason and Marrow (1991) is used. Subsequently,  
83 based on the spatial water distribution, an analytical solution of the NMR diffusion equation  
84 (Torrey, 1956; Brownstein and Tarr, 1979) for partially saturated triangular capillaries is  
85 derived and tested by numerical simulations (Mohnke and Klitzsch, 2010). The derived  
86 equations are used to study the influence of pore size distribution and pore shape of triangular  
87 capillaries on the NMR response, in particular considering the effects of trapped water.  
88 Finally, an approach for simulating NMR signals during imbibition and drainage of triangular  
89 pore capillaries is introduced and demonstrated -using synthetic pore size distributions.

90

## 91 **2 Results and discussion**

### 92 **2.1 Water distribution during drainage and imbibition in a partially saturated**

#### 93 **triangular tube**

94 In a partially saturated pore space, a curved liquid-vapor interface called the arc meniscus  
95 (AM) arises due to the pore's capillary forces. In addition, adsorptive forces between water  
96 and matrix lead to the formation of a thin water film at the rock-air interface. Such water  
97 films with a thickness typically below 20 nm (e.g., Toledo et al., 1990; Tokunaga and Wan,  
98 1997) exhibit very short NMR relaxation times. Although water films to some extent may  
99 influence transport properties and water distribution of a partially saturated porous system  
100 (Tuller and Or, 2001), the contribution of the film volume to NMR amplitudes is very small  
101 with respect to the NMR signal amplitudes arising from the water trapped in the menisci, i.e.,  
102  $V_{\text{film}} \ll V_{\text{meniscus}}$ . Therefore, for sake of simplicity, we neglect water films in his study.

103 In the following discussion, we consider a triangular capillary, initially filled with a  
 104 perfectly wetting liquid, i.e., contact angle  $\theta = 0^\circ$ , which exhibits a constant interfacial  
 105 tension  $\sigma$  ( $\sigma_{\text{air-water}} = 73 \times 10^{-3} \text{ Nm}^{-1}$  at  $20^\circ\text{C}$ ) and is under the assumption that gravity  
 106 forces are weak and therefore can be neglected. The two-phase capillary entry pressure as  
 107 derived by the MS-P method (Mayer and Stowe, 1965; Princen, 1969a, b, 1970) can be  
 108 expressed by the Young-Laplace equation:

$$p_c = \frac{\sigma \cos \theta}{r_{\text{AM}}} = \frac{\sigma}{r_{\text{AM}}}, \quad (1)$$

109 where  $r_{\text{AM}}$  is the radius of the interface arc meniscus and  $p_c$  is the minimum pressure  
 110 difference necessary for a non-wetting fluid-phase, i.e., air, to invade a uniformly wetted (tri-)  
 111 angular tube filled with a denser phase, i.e., water (see Fig. 3a). Upon consideration of a  
 112 pressure difference  $p > p_c$ , the non-wetting fluid-phase will begin to enter the pore and  
 113 occupy the central portion of the triangle, whereas – separated by the three interface arc  
 114 menisci of radius  $r_{\text{AM}}$  – the wetting fluid remains in the pore corners (Fig. 3a).

115 From an original triangle  $ABC$ , a new smaller triangle  $A'B'C'$  of similar geometry with an  
 116 inscribed circle of radius  $r' = r_{\text{AM}} < R_0$  can be constructed by means of the reduced similar  
 117 geometry concept as introduced by Mason and Morrow (1991) (Fig. 3b). To account for  
 118 different transport mechanisms during imbibition and drainage of the denser wetting phase,  
 119 Mason and Morrow (1991) introduced two different principal displacement curvatures with  
 120 radii  $r_I$  and  $r_D$ , respectively.

121 During imbibition of a (tri-)angular pore, the radius of curvature  $r_{\text{AM}}$  increases until the  
 122 separate arc menisci of the corners touch and the pore fills spontaneously (“snap off”). The  
 123 critical radius of curvature  $r_I$ , which is equal to the radius of the pore’s inscribing circle, for  
 124 the angular pore at “snap-off” pressure  $p_I$  is then given by

$$r_I = \frac{2A}{P}, \quad (2)$$

125

126 According to Eq. 2, the snap-off pressure depends on the geometry of the triangle only,  
127 i.e., on its cross-sectional area  $A$  and perimeter  $P$ . In contrast, during drainage the threshold  
128 radius of curvature  $r_D = r_{AM}$ , at which the center of the fully saturated angular capillary  
129 spontaneously empties as a non-wetting fluid phase invades the pore, is given by

$$r_D = P \left[ \frac{1}{2G} + \left( \frac{\pi}{G} \right)^{1/2} \right]^{-1}, \quad (3)$$

130 with  $r_D < r_1$  and drainage threshold pressure  $p_D > p_1$ . The dimensionless and size-  
131 independent factor  $G = \frac{A}{P^2} \left( = \frac{A'}{P'^2} \right)$  reflects the shape of the triangle depending on its cross-  
132 sectional area  $A$  and perimeter  $P$  ( $A'$  and  $P'$  refer to the reduced triangle), i.e., from near-slit-  
133 shape ( $\lim_{\gamma \rightarrow 0} G = 0$ ) to equilateral shape ( $G = 0.048$ ). A detailed derivation of Eqs. 2 and 3  
134 as a consequence of hysteresis between drainage and imbibition can be found in Mason and  
135 Morrow (1991).

136 Note, that the permeability of a porous system of such triangular capillaries is strongly  
137 influenced by the shape factor  $G$ . For single-phase laminar flow in a triangular tube the  
138 hydraulic conductance  $g$  is given by the Hagen-Poiseuille formula

$$g = k \frac{A^2 G}{\mu} \quad (4)$$

139 with the cross-sectional area  $A$ , the shape factor  $G$ , the fluid viscosity  $\mu$ , and  $k$  being a  
140 constant accounting for the geometrical shape of the cross-section, e.g.  $k = 0.5$  for circular  
141 tubes and  $k = 0.6$  for a tube with a cross-section of an equilateral triangle (Patzek and Silin,  
142 2001). The hydraulic conductance of an irregular triangle is closely approximated by  
143 equation 1 using the same constant  $k$  as for an equilateral triangle (Øren et al., 1998). Thus,

144 for a constant cross-sectional area the hydraulic conductance  $g$  of the pore is proportional to  
 145 its shape factor  $G$ .

146 Combining Eqs. 1–3 with the concept of reduced similar geometry discussed above, the  
 147 degree of water saturation ( $S_w$ ) inside a single triangular tube with cross-sectional area  $A_0$ ,  
 148 perimeter  $P_0$ , and radius  $R_0$  of its inscribing circle at a given capillary pressure  $p_c$  during  
 149 imbibition and drainage can be calculated according to  
 150

$$S_w^I(p, A_0, P_0) = \begin{cases} 1 & , p_c \leq p_I \quad (R_0 \leq r_I) \\ \frac{A_\Delta(p_c)}{A_0} & , p_c > p_I \quad (R_0 > r_I) \end{cases} \quad \text{(imbibition)} \quad (5)$$

151

$$S_w^D(p_c, A_0, P_0) = \begin{cases} 1 & , p_c < p_D \quad (R_0 < r_D) \\ \frac{A_\Delta(p_c)}{A_0} & , p_c \geq p_D \quad (R_0 \geq r_D) \end{cases} \quad \text{(drainage)} \quad (6)$$

152

153 The total area  $A_\Delta$  of the triangular tube's water retaining corners,  $\gamma_{1,2,3}$  (i.e., the gray  
 154 areas in Figs. 4 and 5) is expressed by

$$A_\Delta(p_c) = \sum_{i=1}^3 A_{\gamma_i}(p_c), \quad (7a)$$

155 where

$$A_{\gamma_i}(p_c) = \left( \frac{1}{\tan \frac{\gamma_i}{2}} - \frac{(\pi - \gamma_i)}{2} \right) r_{AM}^2(p_c), \quad 0 < \gamma_i < \pi \quad (7b)$$

156 is the area of the triangle's  $i$ th water-filled corner (Tuller and Or, 1999). Consequently, the  
 157 total effective area  $A_\Delta$  still occupied by water is equal to the difference between the (reduced)  
 158 triangular pore area  $\tilde{A}$  and the area  $\pi r_{AM}^2$  of its respective inscribing circle (see Fig. 3). Above

159 equations can be simplified to  $A_{\Delta} = (3\sqrt{3} - \pi) r_{AM}^2(p_c)$  when considering equilateral  
 160 triangles, i.e.,  $\gamma_{1,2,3} = \frac{\pi}{3}$ . The radius  $r_{AM}(p_c)$  of the reduced triangle's arc meniscus can be  
 161 directly calculated from Eq. 1. Calculated pressure-dependent water and gas distributions  
 162 during imbibition and drainage for an equilateral and arbitrary triangular capillary are shown  
 163 in Figs. 4a and 5a. The corresponding water retention curves plotted in Figs. 4b and 5b  
 164 illustrate the resulting hysteresis behavior of the partially saturated system and can be  
 165 subdivided into three parts: at low capillary pressures, i.e.,  $p_c < p_I$ , the pore always remains  
 166 fully water-saturated. For the interval  $p_I < p_c \leq p_D$ , two separate behaviors are observed:  
 167 during imbibition, the water content gradually increases with increasing capillary pressure,  
 168 while during drainage the pore still remains fully saturated. For pressure levels  $p_c \geq p_D$ , both  
 169 drainage as well as imbibition exhibit the same gradual decrease of water saturation.

170 In the following section, analytical solutions for respective NMR responses that arise  
 171 from partially saturated arbitrary triangular tubes are derived and validated with numerical  
 172 simulations of the NMR diffusion equations.

173

## 174 2.2 NMR response for triangular capillaries

175 NMR relaxometry is commonly employed for petrophysical investigations of saturated  
 176 porous rocks in well-logging and laboratory studies. In this respect, the NMR method is a  
 177 unique geophysical tool, which delivers direct information about the water content and allows  
 178 to infer the pore-size distribution in rock samples or the subsurface. The measured NMR  
 179 relaxation signal  $M(t)$  is constituted by superposition of all signal-contributing pores in a rock  
 180 sample (e.g., Coates et al., 1999; Dunn et al., 2002):

$$\frac{M(t)}{M_0} = \frac{1}{V_0} \sum_i^N \left( v_i \times \left( 1 - e^{-t/T_{i,1}^{-1}} \right) \right), \quad (8)$$

181 where  $M_0$  and  $V_0$  are the equilibrium magnetization and total volume of the pore system,  
182 respectively. The saturated volume of the  $i$ th pore and its corresponding longitudinal  
183 relaxation constant are given by  $v_i$  and  $T_{i,1}$ , respectively.

184 Following derivations of Brownstein and Tarr (1979), the inverse of the longitudinal  
185 relaxation time  $T_1$  is linearly proportional to the surface-to-volume ratio of a pore according  
186 to

$$T_1^{-1} = T_{1B}^{-1} + \rho_s \frac{S_a}{V}, \quad (9)$$

187 where  $T_{1B}$  is the bulk relaxation time of the free fluid and  $\rho_s$  is the surface relaxivity, a  
188 measure of how quickly protons ~~lose orientation or phase coherence their magnetization~~ due  
189 to magnetic interactions at the fluid-solid interface, which can be attributed to paramagnetic  
190 ions at mineral grain surfaces.  $V$  and  $S_a$  are the pore's volume and active surface boundaries,  
191 respectively. In this context, an active boundary refers to an interfacial area, i.e., the pore  
192 wall, where  $\rho > 0$  and, thus, enhanced NMR relaxation will occur as the molecules diffuse ~~to~~  
193 at the pore walls. This model, however, is based on the general assumption of a relaxation  
194 regime that is dominated by surface relaxation processes (*fast diffusion*), i.e., the fluid  
195 molecules move sufficiently fast and thus explore all parts of the pore volume with respect to  
196 the time scale ( $\sim T_1$ ) of the experiment.

197 Upon consideration of a long (triangular) capillary, its surface-to-volume-ratio equals its  
198 perimeter-to-cross-section-ratio, i.e.,  $S/V = P/A$ . Consequently, Eq. 9 can be written as

$$T_1^{-1} = T_{1B}^{-1} + \rho \frac{P_0}{A_0}, \quad (10)$$

199 where  $P_0$  is the saturated tube's (active) perimeter and  $A_0$  its cross-sectional area for a circular  
200 cross-section,  $\frac{P_0}{A_0} = \frac{2}{r_0}$ , with  $r_0$  being the capillary radius. Hence, the relaxation rate of a fully  
201 saturated arbitrary triangular pore  $ABC$  can be expressed in terms of its shape factor  $G$  and  
202 perimeter  $P_0$ :

Formatted: Font: Italic



$$T_1^{-1} = T_{1B}^{-1} + \frac{\rho}{G P_0} \left( = T_{1B}^{-1} + \rho \frac{L_{AB} + L_{BC} + L_{CA}}{L_{AB} L_{CA} \sin(\gamma_A)} \right) , \quad (11)$$

203 where  $L_{AB}$ ,  $L_{BC}$ , and  $L_{AC}$  are the lengths of a triangle's sides and  $\gamma_A$  is the angle at corner A  
 204 (see Fig. 3). As illustrated in Fig. 6, the relaxation times of a fully saturated pore decrease  
 205 with decreasing pore shape factor G – and thus, decreasing hydraulic conductance – and  
 206 increasing pore perimeter  $P$ . By reducing one angle from  $60^\circ$  to  $0^\circ$  while fixing another at  
 207  $60^\circ$ , we increase  $P/A$  for a constant cross-sectional area  $A$ . In the special case of an  
 208 equilateral triangular capillary, i.e.,  $P_0/A_0 = \frac{12}{\sqrt{3} L_0}$ , Eq. 11 can be simplified to

$$T_1^{-1} = T_{1B}^{-1} + \rho \frac{12}{\sqrt{3} L_0} . \quad (12)$$

210 Now we consider the previously discussed water-air system of a partially saturated  
 211 equilateral triangular capillary. Here, the NMR signal will originate from the water retained  
 212 at the corners. Replacing  $A_0$  in Eq. 10 with an effective area  $A_\gamma$  or  $A_\Delta$  as derived by Eqs. (7a)  
 213 and b, respectively.  $A_\Delta$  reflects the actual pore fraction that contributes to the NMR signal,  
 214 i.e., the portion of the pore area  $A_0$  that still remains occupied by water.

215 Supposing the air-water interface to be a passive boundary with respect to NMR surface  
 216 relaxivity, i.e.,  $\rho = 0$ , the effective active boundary is exclusively controlled by the pore wall  
 217 segments ( $\rho > 0$ ) in contact with water (wetting phase) (Fig. 7). Thus, the active perimeter of  
 218 such a partially saturated triangular capillary is equal to its pressure-dependent reduced  
 219 triangle's perimeter,  $P'_\Delta(r^{LD}(p_c))$ , according to

$$P_\Delta = \sum_{i=1}^{N=3} P_{\gamma_i} , \quad (13)$$

220 with

Formatted: Font: Not Italic

Formatted: Font: Not Italic

Formatted: Font: Italic

$$P_{\gamma_i} = 2 \frac{r_{AM}(p_c)}{\tan \frac{\gamma_i}{2}}, \quad 0 < \gamma_i < \pi \quad (14)$$

221 being the perimeter of the  $i$ th water-filled corner. Consequently, the NMR relaxation rates  
 222 and NMR signal (amplitude) evolution during drainage and imbibition of a single equilateral  
 223 triangular capillary can be expressed by

$$T_{\Delta,1}^{-1} = \begin{cases} T_{1B}^{-1} + \rho \frac{P_0}{A_0}, & S_w^{I,D} = 1 \\ T_{1B}^{-1} + \rho \frac{P_{\Delta}^{I,D}(p_c, A_0, P_0)}{A_{\Delta}^{I,D}(p_c, A_0, P_0)}, & S_w^{I,D} < 1 \end{cases} \quad (15)$$

225 and

$$\frac{m(t)}{m_0} = S_w^{I,D}(p_c, A_0, P_0) \left( 1 - e^{-\frac{t}{T_{\Delta,1}}} \right), \quad (16)$$

226 respectively. Illustrated in Fig. 8 is the pressure-dependent water distribution inside a single  
 227 equilateral triangular capillary (with a side length of  $1 \mu\text{m}$ ) during drainage (a) and  
 228 corresponding evolution of longitudinal magnetization (b). As the water saturation is reduced  
 229 with increasing pressure, both NMR amplitudes and relaxation times (c) decrease. Note that  
 230 only a single characteristic relaxation time at each saturation degree is observed, since each  
 231 corner has the same  $P_{\gamma}/A_{\gamma}$ , and consequently the same  $T_1$  value.

232 In contrast, each water-filled corner of a partially saturated non-equilateral triangle, i.e.,  
 233  $\gamma_1 \neq \gamma_2 \neq \gamma_3$ , can have a different  $P_{\gamma}/A_{\gamma}$  ratio, and thus will show a different relaxation time  
 234 and amplitude. As a result, depending on its individual shape, even a single partially saturated  
 235 pore exhibits a multi-exponential NMR relaxation behavior based on Eq. (8) according to

$$\frac{m(t)}{m_0} = \frac{1}{A_0} \sum_{i=1}^{N=3} A_{\gamma_i}^{I,D} \left( 1 - e^{-\frac{t}{T_{\gamma_i,1}}} \right), \quad (17)$$

236 with  $T_{\gamma_{i,1}} = \frac{1}{T_{1B}} + \rho \frac{P_{\gamma_i}}{A_{\gamma_i}}$  and  $\frac{A_{\gamma_i}^{1,D}}{A_0}$  being the characteristic relaxation time and amplitude  
 237 contribution of the  $i$ th corner of the triangle, respectively. Figure 9 exemplifies such different  
 238 multi-exponential relaxation behavior for a pore with a right triangle geometry with angles of  
 239 ( $\gamma_1 = 30^\circ, \gamma_2 = 60^\circ, \gamma_3 = 90^\circ$ ) and the same cross-sectional area as the equilateral pores in  
 240 Fig. 8 (i.e.,  $\sim$  NMR porosity).

241 To test the analytical (fast diffusion) models for partially saturated triangular capillaries  
 242 derived above, the calculated longitudinal NMR relaxation times and amplitudes are  
 243 compared to solutions obtained from 2D numerical simulations of the general NMR diffusion  
 244 equation (Mohnke and Klitzsch, 2010):

$$\dot{m} = \left( D \nabla^2 - \frac{1}{T_B} \right) m, \quad (18)$$

245 with normalized initial values  $m(\mathbf{r}, t = 0) = \frac{M_0 - 1}{A}$  and boundary conditions

$$D \mathbf{n} \nabla m \Big|_P = \rho_s m \Big|_P, \quad (19)$$

246 where  $m$  is the magnetization density,  $D$  the diffusion coefficient of water,  $T_B$  the bulk  
 247 relaxation time,  $\rho_s$  the interface's surface relaxivity,  $\mathbf{n}$  the outward normal, and  $A$  and  $P$  the  
 248 pore's cross-sectional area and perimeter, respectively. The above equations were solved  
 249 numerically using finite elements (Mohnke and Klitzsch, 2010) to simulate the respective  
 250 NMR relaxation data of the studied triangular geometries.

251 As shown in Fig. 10, analytically (+) calculated NMR relaxation data for drainage and  
 252 imbibition for an equilateral triangular pore are in a very good agreement ( $R^2 > 0.99$ ) with  
 253 data obtained from numerical simulations (o).

254 The model was also validated for pores with arbitrary angles. Figure 11 illustrates 2D  
 255 finite elements simulations using saturated pore corners with angles  $\gamma_i$  ranging from  $5^\circ$  to  
 256  $175^\circ$  with equal active surface-to-volume ratios  $P_{\gamma_i} / A_{\gamma_i} = \text{const.}$  and thus  $T_{1,i} = \text{const.}$  The

257 simulations were compiled and compared to their respective analytical solutions. The ratios  
258 of the numerical to the analytical model results for NMR amplitudes, i.e., NMR signal  
259 amplitudes,  $A_\gamma$ , and relaxation times,  $T_{1,\gamma}$  as function of corner aperture  $\gamma$  are shown and  
260 confirm a near perfect correlation of  $R^2 > 0.99$ , with deviations generally less than 0.05 %.  
261 In this regard, the slight increase in divergence of relaxation time ratios at acute and obtuse  
262 angles can be attributed to numerical errors resulting from a decrease of the finite element's  
263 grid quality due to extremely high or low x-to-y ratios at these apertures. Note that the above  
264 model is applicable to any angular capillary geometry, such as square or octahedron.

265

### 266 **2.3 Simulated water retention curves and NMR relaxation data of partially saturated** 267 **pore distributions**

268 The goal of this section is to evaluate how pore shape affects the forward-modeled NMR  
269 response of a partially saturated system of pores (a pore size distribution). As discussed  
270 earlier, the NMR relaxation time of a single water-filled capillary pore is inversely  
271 proportional to its surface-to-volume-ratio. Thus at full water saturation, the relaxation-time  
272 distribution obtained from a multi-exponential NMR relaxation signal represents the pore-  
273 size distribution of the rock. At partial water saturation, it is often assumed that the NMR  
274 relaxation signal still represents the pore size distribution of the water saturated pores (e.g.,  
275 Stingaciu, 2010b), which we are going to show is true for the cylindrical but not for (tri-)  
276 angular pores.

277 In contrast to cylindrical pores, capillaries with (tri-)angular cross-sections may be partially  
278 water-saturated during drainage or imbibition (cf. Fig. 8 and 9) because of the water  
279 remaining in the corners. Thus, they show a different water retention behavior and the  
280 “desaturated” pores, i.e. their arc menisci, contribute to the NMR signal. Consequently, with  
281 increasing pressure (i.e. decreasing water saturation) the NMR relaxation behavior of the

282 partially water-saturated triangular capillary pore bundle successively shifts to signal  
283 contributions with shorter relaxation times reflecting the fast relaxation of residual water  
284 trapped in the pore corners (Figure 12). This behavior in angular pore geometries is  
285 demonstrated in Figure 13. Here, the NMR relaxation components for a fully (blue line) and  
286 partially saturated (red and green) distribution of triangular capillaries are plotted. The green  
287 and red peaks show the signals of the residual water in the pore corners. Following from the  
288 reduced geometry concept the remaining water in the corners has the same size and shape,  
289 i.e., the same NMR relaxation time, for all pores independent on their size but dependent on  
290 pressure. Therefore with decreasing saturation, i.e., increasing pressure, the NMR signal of  
291 the arc menisci increases and shifts towards smaller relaxation times. If the non-wetting phase  
292 (air) has entered all capillaries, only one single relaxation time remains for the pore bundle of  
293 equilateral triangles. For arbitrarily shaped triangular pores, three relaxation times would  
294 remain for the de-saturated pore system. Hence, the concept of a relaxation time distribution  
295 assumed in conventional NMR inversion and interpretation approaches would be no longer  
296 valid.

297  
298 All the same, we apply the concept of fitting multi-exponential relaxation time distributions  
299 to NMR transients calculated for pore bundles of circular and equilateral triangle cross-  
300 sections to study how pore shape affects the typically-shown relaxation time distributions.

301 Water drainage and imbibition with water as wetting and air as non-wetting fluid were  
302 investigated by simulating water retention curves and corresponding NMR relaxation signals  
303 for a log-normal distributed pore size ensemble as shown in Figure 14.

304 Herein, to clarify the subsequent discussion we focused on the equilateral triangular  
305 capillary model. Note, that other angular pore shapes (e.g., right angular triangles or squares)  
306 will exhibit a similar behavior. Capillary pressure curves presented in Figure 15a were

307 calculated from -Eq. 1, 4, and 5 for pore bundles with circular and equilateral triangle cross-  
308 sections. In contrast to water retention curves calculated for the cylindrical capillary model  
309 significant hysteresis between drainage and imbibition can be observed for the triangular  
310 capillary model, i.e. in terms of initial amplitudes (=saturation) and respective mean  
311 relaxation times (Figure 15b). -presented water retention curves for drainage and imbibition  
312 were determined from the water distribution inside pores at a stationary states. -Corresponding  
313 NMR  $T_1$  relaxation -(saturation recovery) signals shown in Figure 15c, d and e were  
314 calculated using a uniform surface relaxivity of  $\rho_s = 10 \mu\text{m/s}$  and water bulk relaxation  
315  $T_{1,bulk} = 3 s_2$

316 The NMR  $T_1$  relaxation signals were simulated for 20 saturation levels of the drainage  
317 and imbibition curves ranging from  $S = 100\%$  to  $S < 1\%$  water saturation. The corresponding  
318 relaxation time distributions (Figure 15f-h) of the NMR  $T_1$  transients were determined by  
319 means of a regularized multi-exponential fitting using a nonlinear least squares formulation  
320 solved by the Levenberg-Marquardt approach (e.g., Marquardt, 1963; Mohnke, 2010).  
321 Inverse modeling results of NMR data calculated for the drainage branches using the  
322 cylindrical capillary bundle (Fig. 15f) exhibit a shift of the distribution's maximum towards  
323 shorter relaxation times with decreasing saturation (i.e., increasing pressure). As anticipated,  
324 the derived distribution functions remain inside the envelope of the relaxation-time  
325 distribution curve at full saturation (see also Fig. 1a).

326 In contrast, inversion results for equilateral triangular capillary ensembles (Fig. 15f-h) –  
327 both for imbibition and drainage – show a similar shift to shorter relaxation times with  
328 decreasing saturation but also move outside the initial distribution at full saturation due to  
329 NMR signals originating from trapped water in the pore corners of the desaturated triangular  
330 capillaries. The effect of the pore corners on relaxation time at low saturations is also  
331 recognizable when comparing the (geometric) mean relaxation times, normalized to the

Formatted: Indent: First line: 0"

332 values observed at full saturation (Fig. 15b): Both, the drainage and the imbibition hysteresis  
333 branch of the triangular pore bundle show smaller mean relaxation times than the cylindrical  
334 pore bundle.

335 In conclusion, the calculated inverse models based for ~~on a~~ the triangular capillary bundle  
336 qualitatively agrees with the behavior of the inverted NMR relaxation-time distributions at  
337 partial saturation that are frequently observed in experimental data, e.g., of the Rotliegend  
338 sandstone shown in Fig. 2.

### 339 **3 Summary and conclusions**

340 Experimental NMR relaxometry data and corresponding relaxation-time distributions  
341 obtained at partial water/air saturation were explicated by a modification of conventional  
342 NMR pore models using triangular cross-sections. An analytical solution for calculating  
343 surface-dominated (fast diffusion) NMR relaxation signals in fully and partially saturated  
344 arbitrary angular capillaries ~~, while taking into account residual water trapped in pore corners,~~  
345 was introduced and validated by numerical simulations.

346 Shape and size of triangular pores strongly influence both NMR and flow properties. The  
347 NMR relaxation time depends on the surface-to-volume ratio, which again depends on shape  
348 when considering angular pore capillaries. However, at partial saturation, the pore shape even  
349 more influences the water distribution inside the pore system, and thus the NMR signal. In  
350 contrast to cylindrical capillaries, angular capillaries also contribute to the NMR signal after  
351 desaturation of the pore due to water remaining in the corners.

352 In this regard, non-equilateral triangular capillaries at partial saturation exhibit a three-  
353 exponential relaxation behavior due to different perimeter-to-surface (= surface-to-volume)  
354 ratios of the water in the pore corners whereas the relaxation time of the trapped water in the  
355 corners depends on pressure (but not on pore size).

356 Furthermore, the shape and size of the triangular pores strongly influence both NMR and  
357 hydraulic properties. The NMR relaxation time depends on the surface-to-volume ratio (not  
358 on pore shape), while the water distribution inside the pore system, at partial saturation, is  
359 strongly influenced by the shape of the pore. Thus, the NMR signal at partial saturation is  
360 affected by not only the surface-to-volume ratio, but by the pore shape as well.

361 Moreover, we studied the NMR response of a triangular pore bundle model by jointly  
362 simulating water retention curves for drainage and imbibition and the corresponding NMR  
363  $T_1$  relaxometry data. With decreasing water saturation, the simulated NMR relaxation  
364 distributions shift towards shorter relaxation times below the initial distribution envelope at  
365 full saturation, which is principally in agreement with the relaxation behavior observed in  
366 experimental NMR data from rocks.

367 Ongoing research will include implementation of the introduced approach in an inverse  
368 modeling algorithm for NMR data obtained on partially saturated rocks to predict absolute  
369 and relative permeability at laboratory and borehole scales. Without considering angular  
370 pores the NMR signal of trapped water cannot be explained, i.e., using the classical approach  
371 of circular capillaries one cannot find a pore size distribution which explains the relaxation  
372 time distributions at all saturations sufficiently (e.g., Mohnke, 2014). On the other hand,  
373 angular pore models can account for the trapped water and thus overcome the limitation of  
374 the classical approach. Moreover, following the approach of Mohnke (2014) but considering  
375 angular pores we strive for estimating surface relaxivity, pore size distribution, and pore  
376 shape by jointly inverting NMR data at different saturations. Based on the obtained pore size  
377 distribution and triangle shape we expect to improve the prediction of the absolute and  
378 relative permeabilities considerably.

379



380 **Acknowledgements**

381       The study was supported by the German Research Foundation (DFG) in the framework of  
382 the Transregional Collaborative Research Centre 32 (SFB TR 32) and Wintershall AG in the  
383 framework of Wintershall Tight Gas Consortium at RWTH Aachen University.

384

385 **References**

- 386 Al-Mahrooqi, S. H., Grattoni, C. A., Muggeridge A. H., Zimmermann, R. W., and Jing, X.  
387 D.: Pore-scale modelling of NMR relaxation for the characterization of wettability, J.  
388 Petrol. Sci. Eng., 52, 172–186, 2006.
- 389 Applied Reservoir Technology Ltd.: The NMR Sandstone Rock Catalogue, Long Melford,  
390 Suffolk, U.K., 1996.
- 391 Arnold, J., Clauser, C., Pechinig, R., Anferova, S., Anferov, V., and Blümich, B.: Porosity and  
392 Permeability from Mobile NMR Core-Scanning, Petrophysics, 47, 306–314, 2006.
- 393 [Bird, N.R.A., Preston, A. R., Randall, E. W., Whalley, W.R. and Whitmore, A.P.:  
394 Measurement of the size-distribution of water-filled pores at different matric potentials by  
395 STRAFI-NMR relaxation-time measurements. European Journal of Soil Science. 56: 135-  
396 143, 2005.](#)
- 397 Brownstein, K., and C. Tarr, C. (1979), Importance of classical diffusion in NMR studies of  
398 water in biological cells, Phys. Rev. A, 19, 2446–2453, 1979.
- 399 Chen, S., Liaw, H. K., and Watson, A. T.: Measurements and analysis of fluid saturation-  
400 dependent NMR relaxation and linebroadening in porous media, Magn. Reson. Imaging,  
401 12(2), 201–202, 1994.
- 402 Coates, G. R., Xiao, L., and, Prammer, M. G.: NMR Logging Principles and Applications,  
403 Halliburton Energy Services, Houston, TX, 234 pp., 1999.
- 404 [Costabel, S.: Nuclear magnetic resonance on laboratory and field scale for estimating  
405 hydraulic parameters in the vadose zone, PhD thesis, Berlin University of Technology,  
406 2011. \(opus4.kobv.de/opus4-tuberlin/files/3173/costabel\\_stephan.pdf\)](#) Costabel, S. and  
407 Yaramanci, U.: Relative hydraulic conductivity in the vadose zone from magnetic  
408 resonance sounding - Brooks-Corey parameterization of the capillary fringe, Geophysics,  
409 76(3), G61–G71, doi:10.1190/1.3552688, 2011.

410 Costabel, S. and Yaramanci, U.: Estimation of water retention parameters from nuclear  
411 magnetic resonance relaxation time distributions, *Water Resour. Res.*, 49(4), 2068–2079,  
412 doi:10.1002/wrcr.20207, 2013.

413 Desbois, G., Urai, J. L., Kukla, P. A., Konstanty, J., and Baerle, C.: High-resolution 3D fabric  
414 and porosity model in a tight gas sandstone reservoir: A new approach to investigate  
415 microstructures from mm- to nm-scale combining argon beam cross-sectioning and SEM  
416 imaging, *J. Petrol. Sci. Eng.*, 78, 243–257, doi:10.1016/j.petrol.2011.06.004, 2011.

417 Dong, M. and Chatzis, I.: The imbibition and flow of a wetting liquid along the corners of a  
418 square capillary tube, *J. Colloid Interface Sci.*, 172, 278–288, 1995.

419 Dunn K. J., Bergman D. J., and LaTorraca G. A.: Nuclear Magnetic Resonance:  
420 Petrophysical and Logging Applications, Pergamon: Elsevier Science, Amsterdam, 2002.

421 Finjord, J., Hiorth, A., a Lad, U. H., and Skjaeveland, S. M.: NMR for equilateral triangular  
422 geometry under conditions of surface relaxivity - analytical and random walk solution,  
423 *Transport Porous Med.*, 69, 33–53. arXiv:cond-mat/0508412v2, 2006.

424 Fleury, M., Deflandre F., and Godefroy, S.: Validity of permeability prediction from NMR  
425 measurements, *CR. Acad. Sci. Series IIC – Chemistry*, 4, 869–872, doi:10.1016/S1387-  
426 1609(01)01343-3, 2001.

427 Ioannidis, M., Chatzis, I., Lemaire, C., and Perunarkilli, R.: Unsaturated hydraulic  
428 conductivity from nuclear magnetic resonance measurements, *Water Resour. Res.*, 42(7),  
429 [W07201](#), [6 pages](#), doi:10.1029/2006WR004955, 2006.

430 [Jaeger, F., Bowe, S., van As, H., and Schaumann, G. E. \(2009\). Evaluation of 1 H NMR](#)  
431 [relaxometry for the assessment of pore size distribution in soil samples. \*European Journal of\*](#)  
432 [Soil Science, 60:1052 – 1064.](#)

433 Jia, P., Dong, M., and Dai, L.: Threshold pressure in arbitrary triangular tubes using RSG  
434 concept for all wetting conditions, *Colloid. Surface A*, 302, 88–95, 2007.

**Comment [A1]:** This is the article number

435 Kenyon, W.: Petrophysical principles of applications of NMR logging, *Log Anal.* 38(2), 21–  
436 43, 1997.

437 Kleinberg, R.L.: Utility of NMR T2 distributions, connection with capillary pressure, clay  
438 effect, and determination of the surface relaxivity parameter  $\rho_2$ , *Magn. Reson. Imaging*,  
439 14(7), 761–767. doi: 10.1016/S0730-725X(96)00161-0, 1996.

440 Lenormand R., Zarcone C., Sarr, A.: A Mechanisms of the displacement of one fluid by  
441 another in a network of capillary ducts, *J. Fluid Mech.*, 135, 337–353, 1983.

442 Liaw, H.-K., Kulkarni, R., Chen, S., and Watson, A.T.: Characterization of fluid distributions  
443 in porous media by NMR techniques, *AIChE J.*, 42(2), 538–546, doi:  
444 10.1002/aic.690420223, 1996.

445 Marquardt, D. W.: An Algorithm for the Least-Squares Estimation of Nonlinear Parameters,  
446 *Siam J. Appl. Math.*, 11(2), 431–441, 1963.

447 Mason, G. and Morrow, N. R.: Capillary behavior of a perfectly wetting liquid in irregular  
448 triangular tubes, *J. Colloid. Interf. Sci.*, 141, 262–274, 1991.

449 Mayer, R. P., and Stowe, R. A.: Mercury porosimetry-breakthrough pressure for penetration  
450 between packed spheres, *J. Colloid. Interf. Sci.*, 20, 893–911, 1965.

451 Mohnke, O.: Improved forward and inverse modelling of Surface NMR relaxation signals  
452 using multi-exponential decomposition, Ph.D. thesis, Technical University Berlin, [Berlin](#),  
453 2010.

454 Mohnke, O. and Klitzsch, N.: Microscale Simulations of NMR Relaxation in Porous Media  
455 Considering Internal Field Gradients, *Vadose Zone J.*, 9, 846–857,  
456 doi:10.2136/vzj2009.0161, 2010.

457 [Øren, P. E., S. Bakke, and O. J. Arntzen. Extending predictive capabilities to network](#)  
458 [models, \*SPE Journal\*, 3, 324-336, 1998.](#)

459 Or, D. and Tuller, M.: Flow in unsaturated fractured porous media: Hydraulic conductivity of  
460 rough surfaces. *Water Resour. Res.*, 36(5), 1165–1177, doi:10.1029/2000WR900020,  
461 2000.

462 [Patzek, T. W., and D. B. Silin, Shape factor and hydraulic conductance in noncircular](#)  
463 [capillaries I. One-phase creeping flow, \*Journal of Colloid and Interface Science\*, 236,](#)  
464 [295-304, 2001.](#)

465 Princen, H. M.: Capillary phenomena in assemblies of parallel cylinders I. Capillary rise  
466 between 2 cylinders, *J. Colloid. Interf. Sci.*, 30, 69–75, 1969a.

467 Princen, H. M.: Capillary phenomena in assemblies of parallel cylinders II. Capillary rise in  
468 systems with more than 2 cylinders, *J. Colloid. Interf. Sci.*, 30, 359–371, 1969b.

469 Princen, H. M.: Capillary phenomena in assemblies of parallel cylinders III. Liquid columns  
470 between horizontal parallel cylinders, *J. Colloid. Interf. Sci.*, 34, 171–184, 1970.

471 Ransohoff, T. C., and Radke, C. J.: Laminar flow of a wetting liquid along the corners of a  
472 predominantly gas-occupied noncircular pore, *J. Colloid Interface Sci.*, 121, 392–401,  
473 1987.

474 Seevers, D. O.: A nuclear magnetic method for determining the permeability of sandstones,  
475 Society of Professional Well Log Analysts, vol. 6, paper L, [Houston, Texas](#), 1966.

476 Stingaciu, L. R.: Characterization of natural porous media by NMR and MRI techniques:  
477 High and low magnetic field studies for estimation of hydraulic properties, Ph.D. thesis,  
478 RWTH Aachen, URL: <http://darwin.bth.rwth-aachen.de/opus3/volltexte/2010/3392/>,  
479 2010a ([accessed on 06/30/2014](#)).

480 Stingaciu, L. R., Weihermüller, L., Haber-Pohlmeier, S., Stapf, S., Vereecken, H., and  
481 Pohlmeier, A.: Determination of pore size distribution and hydraulic properties using  
482 nuclear magnetic resonance relaxometry: A comparative study of laboratory methods.  
483 *Water Resour. Res.*, 46, 1–11, doi:10.1029/2009WR008686, 2010b.

Formatted: Indent: Left: 0",  
Hanging: 0.25"

484 Talabi, O., AlSayari, S. Iglauer, I., and Blunt, J.: Pore-scale simulation of NMR response, J.  
485 Petrol. Sci. Eng., 67, 168–178, 2009.

486 [Thern, H.: Examining the fluid film model in porous media by NMR rock catalogue data,](#)  
487 [Symposium of the Society of Core Analysts, Avignon, France, paper SCA2014-051.](#)

488 Tokunaga, T. K. and Wan, J.: Water film flow along fracture surfaces of porous rock, Water  
489 Resour. Res., 33(6), 1287–1295, doi:10.1029/97WR00473, 1997.

490 Toledo, P. G., Novy, R. A., Davis, H. T., and Scriven, L. E.: Hydraulic Conductivity of  
491 Porous Media at Low Water Content, Soil Sci. Soc. Am. J., 54, 673–679,  
492 10.2136/sssaj1990.03615995005400030007x, 1990.

493 Torrey, H. C.: Bloch equations with diffusion terms, Phys. Rev., 104(3), 563–565,  
494 doi:10.1103/PhysRev.104.563, 1956.

495 Tuller, M., Or, D., and Dudley, L.M.: Adsorption and capillary condensation in porous media  
496 - liquid retention and interfacial configurations in angular pores, Water Resour. Res.,  
497 35(7), 1949–1964, doi: 10.1029/1999WR900098, 1999.

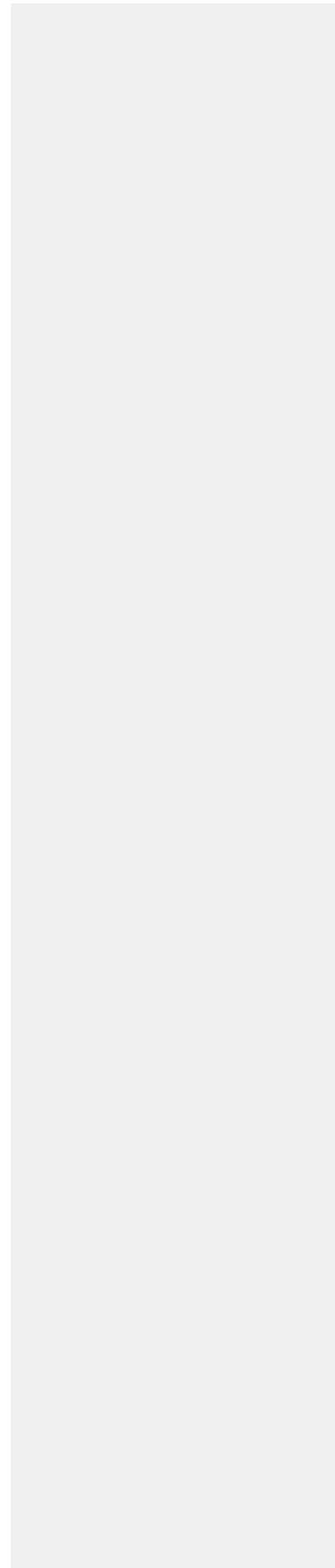
498 Tuller, M. and Or, D.: Hydraulic conductivity of variably saturated porous media: Film and  
499 corner flow in angular pore space, Water Resour. Res., 37(5), 1257–1276, [DOI:](#)  
500 [10.1029/2000WR900328](#)~~doi:10.1029/2000WR900~~, 2001.

501

Formatted: Indent: Left: 0",  
Hanging: 0.25"

502      FIGURES

503



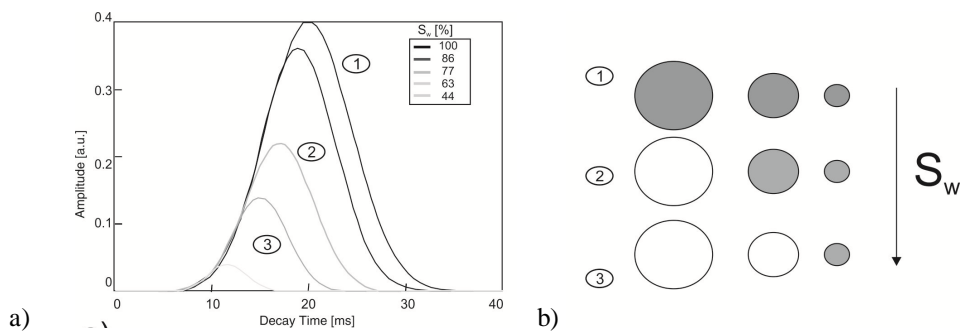
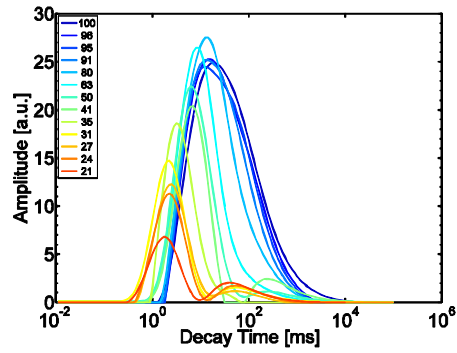
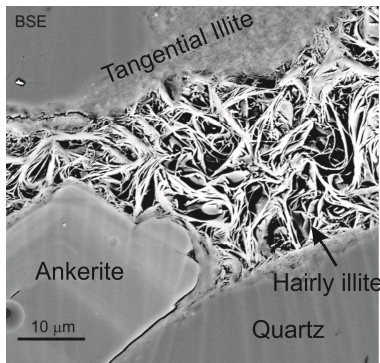


**Figure 1.** a) NMR decay time distributions at different water saturation levels for a classical cylindrical capillary pore distribution. b) Concept sketch of saturated (gray) and de-saturated capillaries, e.g., during drainage.

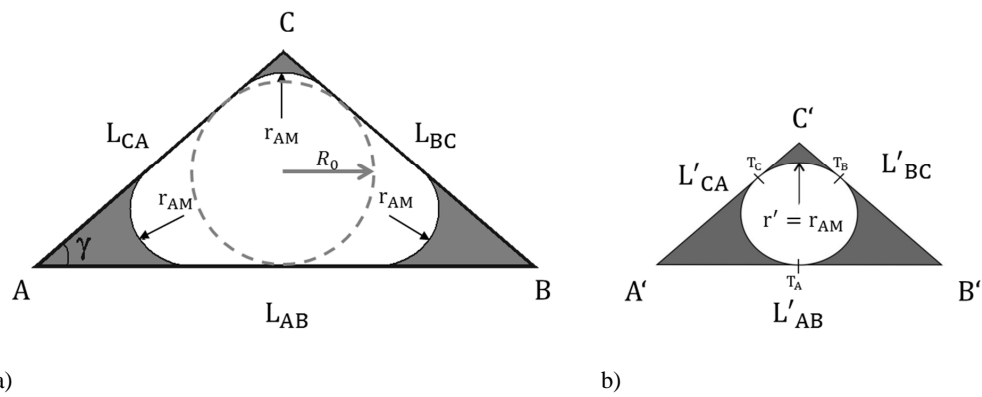




a)

b)

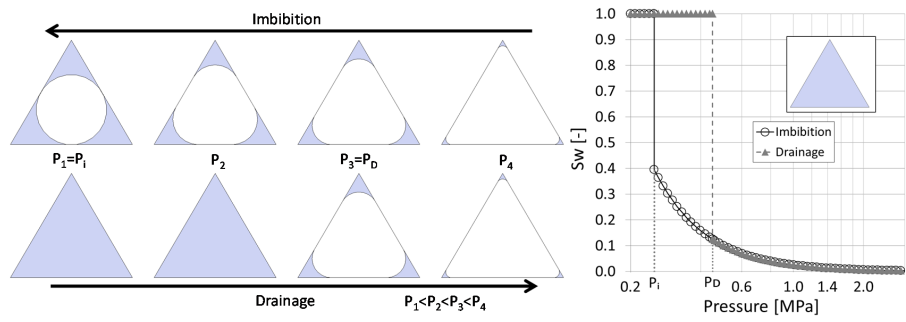
**Figure 2.** a) Complex pore structure of a Rotliegend tight gas sandstone. Pore spaces are filled with tangential and hairy illite and exhibit different pore types with elongated or slit-shaped, triangular, and multi-angular cross-sections. b)  $T_1$  decay time distributions calculated from inverse Laplace transform performed on Rotliegend sandstone (porosity 13%, permeability 0.1 mD) at different water saturations ( $S_w = 21\% - 100\%$ ).



a) Original triangle  $ABC$  with side lengths  $L_{AB}, L_{BC}, L_{CA}$ , and radius  $R_0$  of its inscribing circle.  
 b) Reduced triangle  $A'B'C'$  of similar geometry. The wetting phase resides in the three corners (gray) with  $r' = r_{AM}$  being the radius of both the three interface arc menisci of  $ABC$  and of the inscribing circle of  $A'B'C'$

506

507



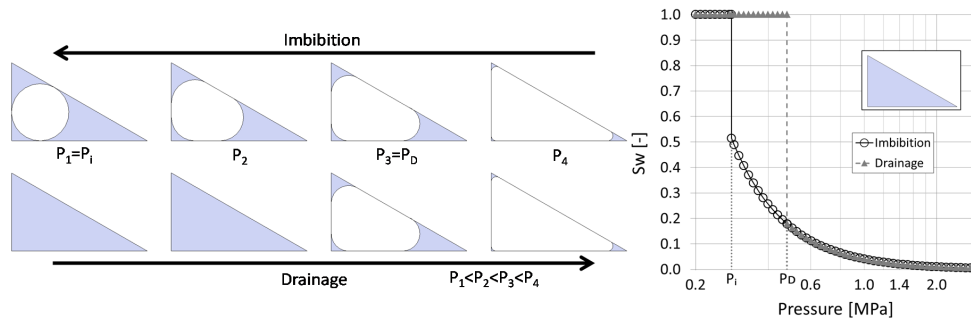
a)

b)

**Figure 4.** a) Modeled distribution of water (gray) and gas (white) phases in an equilateral triangular tube with a side length of  $1 \mu\text{m}$  during imbibition (top) and drainage (bottom). b) Water saturation versus capillary pressure during imbibition ( $\circ$ ) and drainage ( $\blacktriangle$ ).

508

509



a)

b)

**Figure 5.** a) Modeled distribution of water (gray) and gas (white) phases in a right-angled triangular capillary ( $G = 0.39$ ) with side lengths  $L = 1, 0.81, 0.58 \mu\text{m}$ , and perimeter  $P = 2.39 \mu\text{m}$  during imbibition (top) and drainage (bottom). b) Water saturation versus capillary pressure during imbibition ( $\circ$ ) and drainage ( $\blacktriangle$ ).

510

511

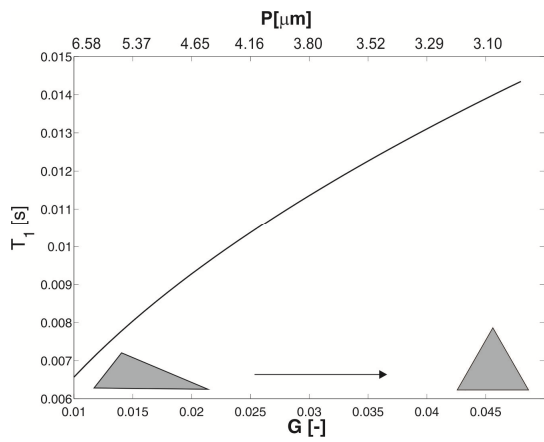


**Figure 6.** Longitudinal relaxation times  $T_1$  of fully saturated triangular pores with constant cross-sectional area  $A = 4.33 \cdot 10^{-13} \text{ m}^2$  versus shape factor  $G = \frac{A}{p^2}$  and perimeter  $P$ . NMR parameters:  $\rho_s = 10 \frac{\mu\text{m}}{\text{s}}$ ,  $T_{1B} = 3 \text{ s}$ .

512

513

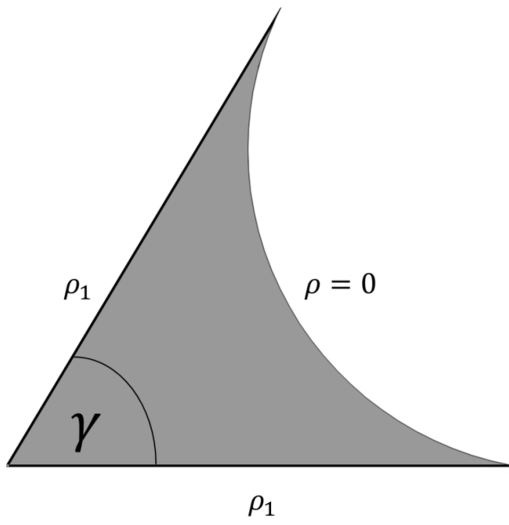


**Figure 7.** Saturated corner with active boundaries, i.e.,  $\rho_s = \rho_1 > 0$  at the corner's perimeter  $P_\gamma$  and a passive boundary at the air-water interface (meniscus), i.e.,  $\rho_s = \rho = 0$ .

514

515

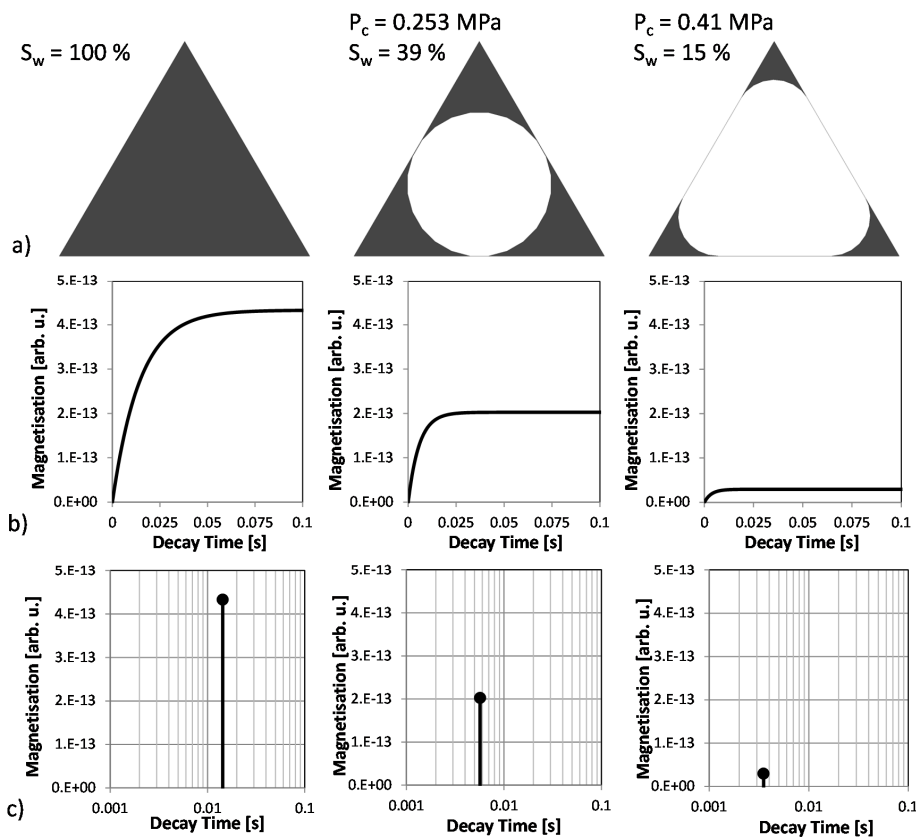


**Figure 8.** Water (black) and air (white) distributions within a triangular pore ( $A_0 = 4.33 \cdot 10^{-13} \text{ m}^2$ ,  $\rho_s = 10^{-5} \text{ m/s}$ ) at different capillary pressures for imbibition (a) with corresponding evolution of the (longitudinal) magnetization (b) and NMR  $T_1$  relaxation times (c).

516

517

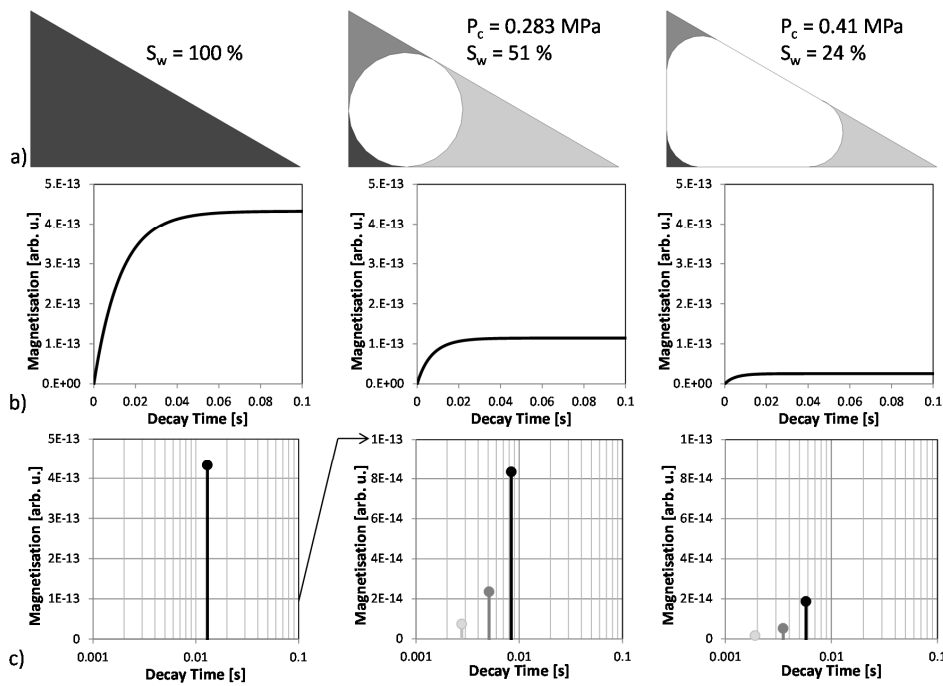


**Figure 9.** Water (black and grays) and air (white) distributions within a right-angled triangular pore ( $A_0 = 4.33 \cdot 10^{-13} \text{ m}^2$ ,  $\rho_s = 10^{-5} \text{ m s}^{-1}$ ) at different capillary pressures for imbibition (a) with corresponding evolution of the (longitudinal) magnetization (b) and NMR  $T_1$  relaxation times (c).

518

519



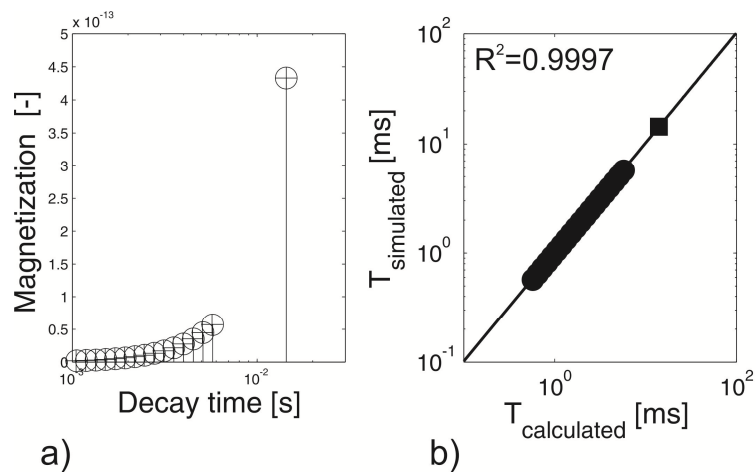


**Figure 10.** NMR response of an equilateral triangular capillary pore model (with a side length of  $1 \mu\text{m}$ ). a) Magnetization versus  $T_1$  decay time data of numerical ( $\circ$ ) and analytical solutions ( $+$ ) for all applied pressure levels. b) Cross-plot of numerically simulated and analytically calculated longitudinal  $T_1$  decay-times at partial ( $\bullet$ ) and full water saturation ( $\blacksquare$ ). A corresponding water saturation versus capillary pressure diagram is shown in Fig. 4.

520

521

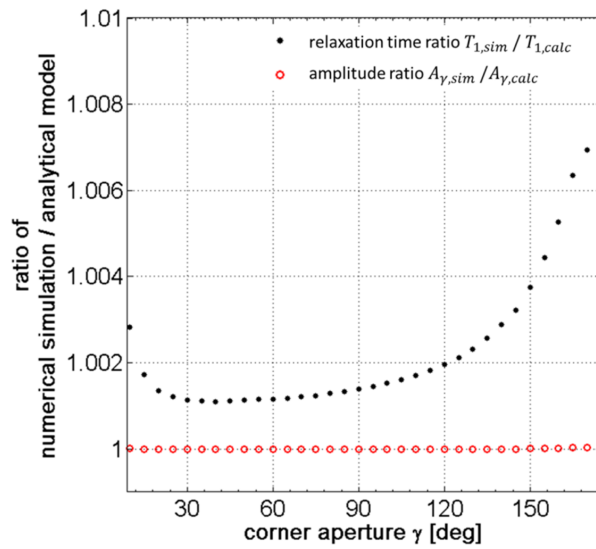
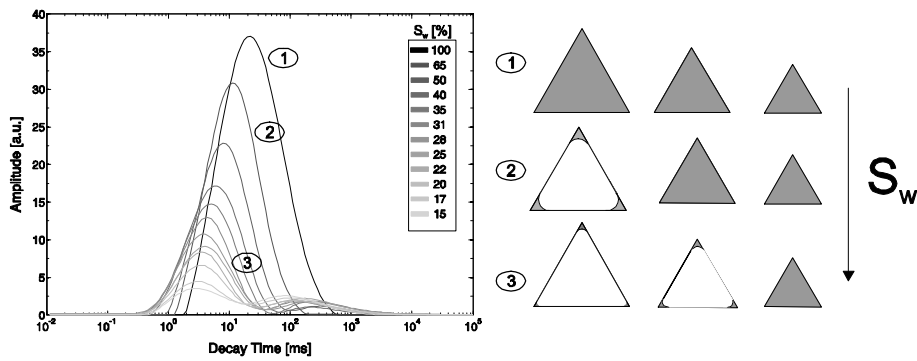


**Figure 11.** Comparison of analytical and calculated NMR relaxometry data originating from saturated pore corners (e.g. see Fig. 7) of varying apertures ( $5^\circ < \gamma < 175^\circ$ ) and equal active surface-to-volume ratio  $\frac{P_{\gamma i}}{A_{\gamma i}} = const.$  (NMR model parameters;  $T_{1B} = 3\text{ s}$ ,

$$D = 2.5 \cdot 10^{-9} \text{ m}^2 \text{ s}^{-1}, \rho_s = 10 \mu\text{m s}^{-1}).$$

522

523



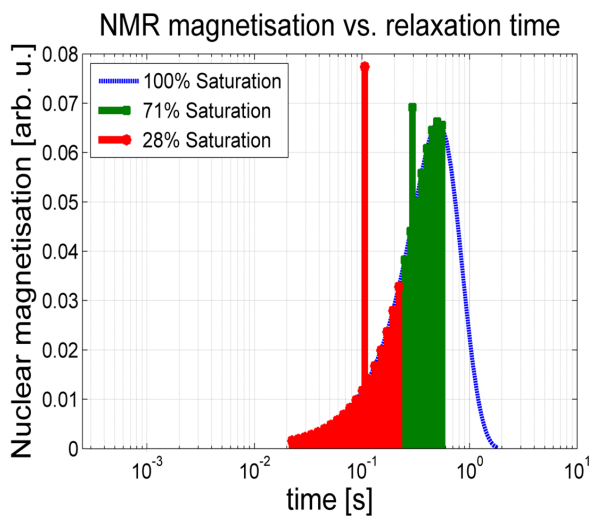
a)

b)

**Figure 12.** a) NMR decay time distributions at different water saturation levels for a pore distribution of equilateral triangles. b) Concept sketch of saturated (gray) and de-saturated triangular capillaries for increasing pressure levels (1), (2) and (3), e.g., during drainage.

524  
525

**Formatted:** Indent: First line: 0.25",  
Space After: 6 pt, Line spacing: 1.5  
lines, Tab stops: 0.25", Left + 5.12",  
Right + 6.2", Right



Formatted: Centered

Formatted Table

Figure 13: Relaxation components of fully (blue line) and partially de-saturated triangular pore size distribution. At a specific saturation level all pore corners with residual saturation exhibit the same NMR magnetization and relaxation behavior, thus superposing to a single fast relaxation component (e.g. red and green bars)

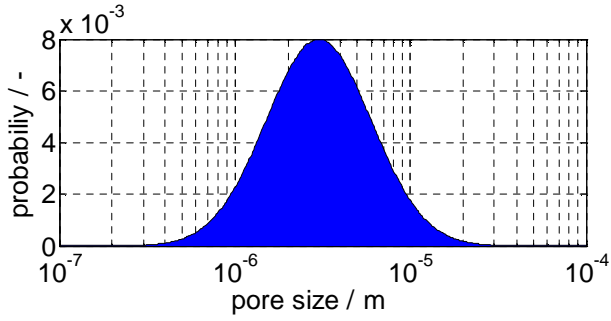


Figure 14. Pore-size distribution model (log-normal distribution:  $\sigma = 0.3, \mu = 3 \mu\text{m}$ ) in analogy to that of the Rotliegend Sandstone shown in Fig. 2.

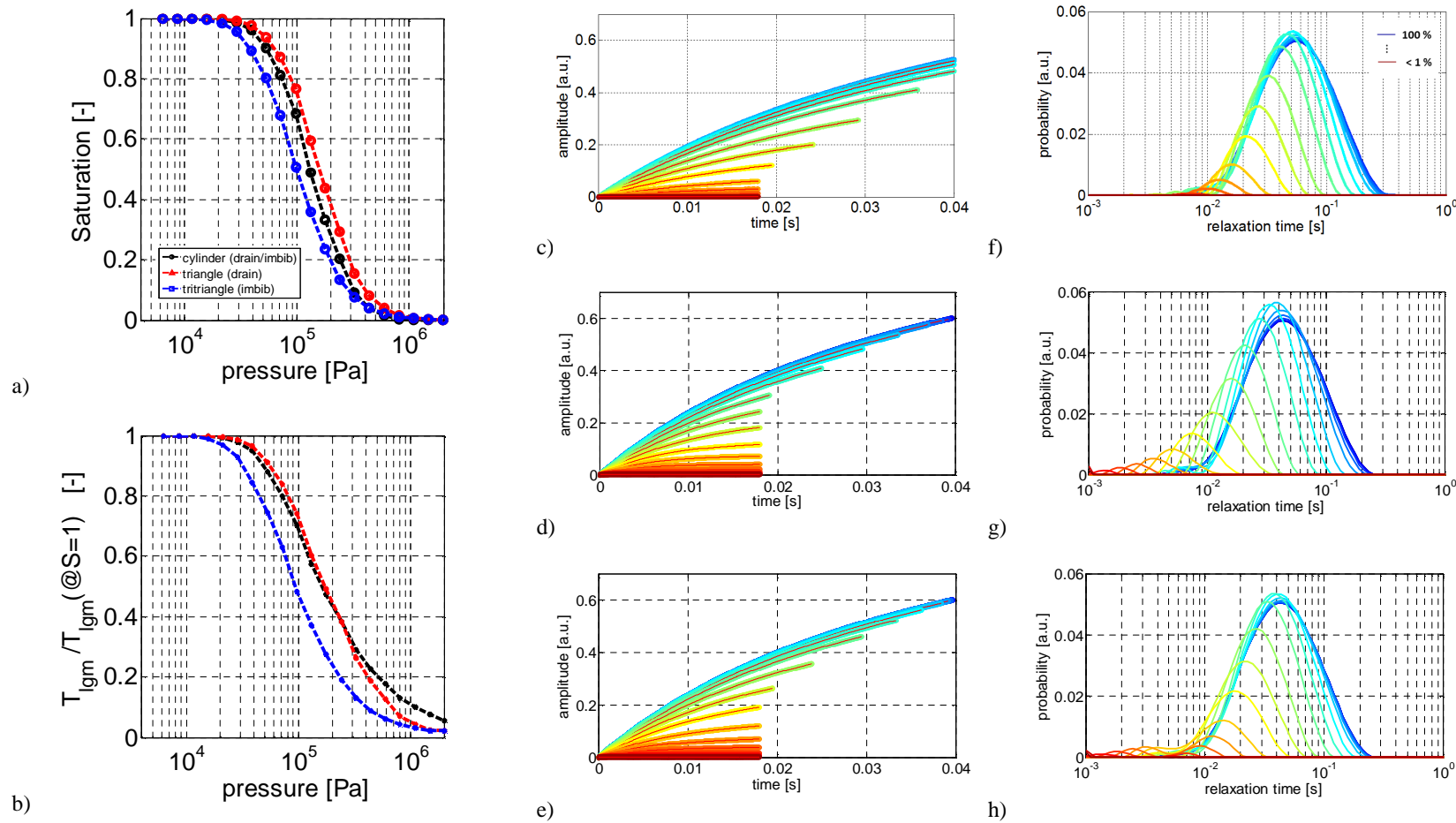


Figure 15: a) Modeled drainage and imbibition curves for circular and equilateral triangular capillary ensemble (cf Figure 14) and b) Corresponding normalized mean NMR  $T_1$  relaxation times vs pressure curves. Modeled and fitted (red lines) NMR transient signals (longitudinal magnetization evolution) corresponding inverted NMR  $T_1$  relaxation time distributions for 20 fully and partially saturated pore-size distributions ranging from < 1 % to 100 % saturation using circular (c, f) and equilateral triangular capillaries during imbibition (d, g) and drainage (e, h).

